Letter

In silico testing of the universality of epithelial tissue growth

Mahmood Mazarei,[1] Jan Åström,[2] Jan Westerholm,[3] and Mikko Karttunen[1,4]

[1]*Department of Physics and Astronomy, Western University, 1151 Richmond Street, London, Ontario, Canada N6A 3K7*

[2]*CSC Scientific Computing Limited, Kägelstranden 14, FI-02150 Esbo, Finland*

[3]*Faculty of Science and Engineering, Åbo Akademi University, Vattenborgsvägen 3, FI-20500 Åbo, Finland*

[4]*Department of Chemistry, Western University, 1151 Richmond Street, London, Ontario, Canada N6A 5B7*

(Received 29 March 2022; accepted 22 November 2022; published 12 December 2022)

The universality of interfacial roughness in growing epithelial tissue has remained a controversial issue. Kardar-Parisi-Zhang (KPZ) and molecular beam epitaxy (MBE) universality classes have been reported among other behaviors including a total lack of universality. Here, we simulate tissues using the CELLSIM3D kinetic division model for deformable cells to investigate cell-colony scaling. With seemingly minor model changes, it can reproduce both KPZ- and MBE-like scaling in configurations that mimic the respective experiments. Tissue growth with strong cell-cell adhesion in a linear geometry is KPZ like, while weakly adhesive tissues in a radial geometry are MBE like. This result neutralizes the apparent scaling controversy.

DOI: 10.1103/PhysRevE.106.L062402

Introduction. The growth of biological matter, e.g., tumor invasion, depends on complex processes such as the mechanism(s) of proliferation, the physical properties of the microenvironment, and cellular migration that can be dominated either by single-cell or collective motion [1]. Numerous experimental and computational studies have investigated the effects of biochemical regulation and mechanical factors such as cell-to-cell adhesion and friction, and cell division [2–11]. To understand how these factors manifest in terms of both kinetics and morphology, the interfacial growth of a tissue can be characterized by a scaling analysis. This, in turn, identifies governing equations and hence leading-order behavior(s).

Often, the interface width $w(l,t)$ obeys the Family-Vicsek scaling relation [12,13]

$$w(l,t) \sim t^{\beta} F(lt^{-\frac{1}{z}}), \tag{1}$$

where the exponent z describes the scaling relation between the critical time and length scales, and can be obtained from the scaling relation $z = \frac{\alpha}{\beta}$, where the exponent α characterizes the roughness of the interface. The exponent β is obtained through the scaling function $F(u) = F(lt^{-\frac{1}{z}})$ which has the following properties: There is a crossover at $u = l_*$. For $u \ll l_*$ the scaling function increases as a power law, $F(u) = u^{\alpha}$ where α is the roughness exponent. For $u \gg l_*$ the width saturates, and $F(u)$ becomes a constant [14]. With these three critical exponents, α, β, and z, interfacial growth is often classified into different dynamic universality classes.

The Kardar-Parisi-Zhang (KPZ) equation is a stochastic nonlinear differential equation for surface growth [15],

$$\partial_t h(x,t) = -\lambda[\partial_x h(x,t)]^2 + \nu \partial_x^2 h(x,t) + \xi(x,t), \tag{2}$$

where the height $[h(x,t)]$ depends on position and time, and λ, ν, and D are physical constants. The first term on the right-hand side reflects growth that occurs locally normal to the interface and renders the KPZ equation nonlinear. The second term smooths the interface by surface tension ν, and the last term, $\xi(x,t)$, is Gaussian noise given by $\langle \xi(x,t) \rangle = 0$ and $\langle \xi(s,x)\xi(t,y) \rangle = 2D\delta(s-t)\delta(x-y)$. The KPZ universality class is characterized by the exponents $\alpha^{\mathrm{KPZ}} = \frac{1}{2}$, $\beta^{\mathrm{KPZ}} = \frac{1}{3}$, and $z^{\mathrm{KPZ}} = \frac{3}{2}$ [15].

Mathematically, surface tension and lateral growth determine the asymptotic scaling of the KPZ equation. In some growth processes, however, surface diffusion controls the scaling behavior, and the growth process is described by the molecular beam epitaxy (MBE) model [16,17]

$$\partial_t h(x,t) = -K\partial_x^4 h(x,t) + F + \xi(x,t), \tag{3}$$

where K is the surface diffusion coefficient, F is the growth rate, and $\xi(x,t)$ is Gaussian white noise. The exponents for the MBE universality class for a one-dimensional interface are $\alpha^{\mathrm{MBE}} = \frac{3}{2}$, $\beta^{\mathrm{MBE}} = \frac{3}{8}$, and $z^{\mathrm{MBE}} = 4.0$.

Apparent controversy. Brú *et al.* studied cellular growth using cells from 15 different *in vitro* cell lines and 16 *in vivo* types of tumor cells obtained from patients [7,8]. They determined the growth to belong to the MBE universality class in all cases with exponents $\alpha = 1.5 \pm 0.15$, $\beta = 0.38 \pm 0.07$, and $z = 4.0 \pm 0.5$, thus suggesting universal growth dynamics for cells. This conclusion was strongly criticized by Buceta and Galeano [18], who dismissed the universality of tumor growth dynamics stating serious flaws in Brú *et al.*'s scaling analysis. In their rebuttal, Brú *et al.* [9] restated their conclusions and wrote "the characteristics of MBE dynamics discussed in Brú *et al.* (2003, 1998) have not only been rigorously demonstrated but have served as the basis for a successful antitumor therapy currently under development." A recent study of the growth of different brain tumors *in vivo* using fractal and scaling analysis shows similarities with some of the results of Brú *et al.* [19].

In contrast to MBE-like dynamics, Huergo *et al.* [10,11,20] reported KPZ scaling for both linearly and radially spreading interfaces of HeLa (cervix cancer) and Vero cell colonies. Galeano *et al.* studied the development of plant cell species *Brassica oleracea* and *B. rapa* under various growing conditions and obtained $\alpha = 0.86 \pm 0.4$, and $z = 5.0$ [21]. Santalla *et al.* [22] grew colonies of *B. subtilis* and *E. coli* using a high agar concentration regime with various nutrients and discovered branching interfaces with exponents $\beta = 0.5$ and $\alpha = 0.75$ that are inconsistent with both MBE and KPZ.

Substrate disorder can also influence growth dynamics. Vicsek *et al.* [23] studied the growth of *E. coli* and *B. subtilis* colonies and found the roughness exponent $\alpha = 0.78 \pm 0.07$ which is inconsistent with both the KPZ and MBE models as well as with the quenched KPZ (qKPZ) model [14] that includes disorder. It has also been demonstrated that the behavior of bacterial colonies in the medium-to-high nutrient concentration regime can be very rich due to the appearance of quenched disorder in growth patterns [24]. In that context, Huergo *et al.* also examined the two-dimensional (2D) growth dynamics of quasilinear Vero cell-colony fronts in a methylcellulose-containing culture medium. Their scaling analysis yielded $\alpha = 0.63 \pm 0.04$, $\beta = 0.75 \pm 0.05$, and $z = 0.84 \pm 0.05$, suggesting qKPZ dynamics [25].

On the computational and theoretical side, Santalla and Ferreira [26] used an off-lattice Eden model modified to account for nutrient diffusion. Under scarce nutrient supply, they observed initially a KPZ regime that transitioned via a qKPZ transient to unstable growth. Block *et al.* studied the growth of 2D cellular monolayers for a class of cellular automaton models. Their results suggest KPZ dynamics over a wide range of parameters and different cell migration dynamics [27] contradicting the MBE dynamics reported by Brú *et al.* [7]. Another contradiction was reported by Azimzade *et al.* who developed a tumor growth model based on the nonlinear Fisher-Kolmogorov-Petrovsky-Piskunov equation, a reaction-diffusion equation, to investigate the impact of the cellular environment and spatial correlations on tumor invasion [28]. They concluded that kinetic growth models, such as KPZ, cannot characterize tumor invasion fronts, and that the structure of the tumor interface depends intimately on the initial conditions [28].

Simulations. A large number of different models has been used to describe cellular growth [29]. Here, we use the CELLSIM3D off-lattice growth model and simulator to study epithelial tissue growth [30,31]. In this model, cells can migrate, deform, divide, and interact with each other and their environment mechanically via adhesion and friction. Its 2D version has been shown to produce, e.g., cell-cell force distributions, force dipoles, spontaneous orientation of cells in the direction of highest stiffness, and cellular migration in agreement with experiments [32]. The analysis below uses averages over ten independent simulations. In brief, in CELLSIM3D, epithelial tissues can be modeled as quasi-2D systems of 3D cells confined into a plane, corresponding to the experimental confinement of cells between two plates; the bottom plate models basal tissue and the top plate prevents excessive buckling. Details of the code, model, and parameters are provided in the Supplemental Material [33]. The code is open source [34].

Interface scaling. The interface width is defined as the standard deviation of height over a length scale l at time t as [14]

$$w(l,t) = \left\{ \frac{1}{N} \sum_{i=1}^{N} [h_i(t) - \langle h_i \rangle_l]^2 \right\}_L^{\frac{1}{2}}, \tag{4}$$

where L is the contour length, which increases with time as $L = 2\pi \langle h(t) \rangle$ for radially expanding fronts and is constant for linear fronts. For radially expanding fronts, $h_i(t)$ is the distance from the center of mass to the point i of the interface at time t, $\langle h_i \rangle_l$ is the local average of the subsets of arc length l, and $\{\cdot\}_L$ is the overall average. We complement the universality class analysis by an examination of the structure factor,

$$S(k,t) = \langle \hat{h}(k,t) \hat{h}(-k,t) \rangle, \tag{5}$$

where k is the wave number, and $\hat{h}(k,t)$ is the Fourier transform of the interface profile $h(x,t)$ [14]. The advantage of the Fourier method over the real space method is that only long-wavelength modes contribute to its scaling. Hence, it is less affected by finite-size effects. This method provides the global roughness exponent α and the dynamic exponent z via the Family-Vicsek scaling form [Eq. (1)] for $S(k,t)$,

$$S(k,t) = k^{-(2\alpha+1)} s(kt^{\frac{1}{z}}), \tag{6}$$

where

$$s(u = kt^{\frac{1}{z}}) = \begin{cases} \text{const} & \text{for } u \gg 1, \\ u^{2\alpha+1} & \text{for } u \ll 1. \end{cases} \tag{7}$$

At $u = 1$ there is a crossover, for $u \gg 1$ the curves measured at different times collapse, and for $u \ll 1$ they split.

We first consider the growth of linear fronts at two different adhesion strengths, 10 (weak) and 2000 (strong) (see Table S1 for parameters). The initial configurations had a line of 240 cells, and the final populations consisted of ≈200 000 cells. Snapshots are shown in Fig. 1. As this figure shows, increasing the cell-cell adhesion changes the morphology of the colony and the interface. Figure 2(a) shows that the interfaces grow at constant velocities with the growth rate decreasing with increasing adhesion.

Next, the box counting method was utilized to determine the fractal dimensions (d_f) of the interfaces for both line configurations (triangles) and radially growing (circles) systems. Figure 2(b) shows that d_f is in the same range for all simulations. In both geometries, however, d_f is slightly higher for the case of strong adhesion. This is consistent with the experiments of Torres Hoyos *et al.* [19] who reported smaller d_f for malignant and invasive cancer cells as compared to the benign and more solid (higher adhesion) tumors.

We investigate the scaling behavior by plotting the width scaling function $F(u)$ in Eq. (1) and the structure scaling function $s(u)$ in Eq. (6) at three different time points in order to see if they collapse for given values of α, β, and z. Instead of relying only on a visual inspection, we calculated the chi-squared statistics [Eq. (S12)] similar to the concept of the maximum likelihood estimator for equality of two distributions. Figures 3(a)–3(d) show the scaling results for line growth both via the width function [Eq. (1)] and the structure

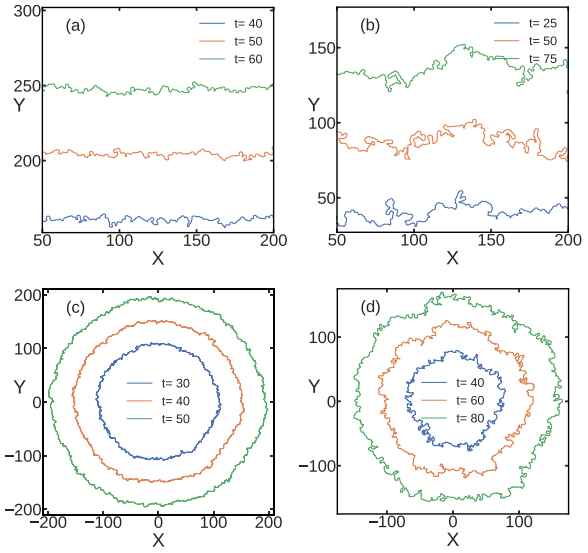

FIG. 1. Interface evolutions of cell colonies starting from a horizontal line and a radially expanding interface. (a) Line configuration at weak (10) and (b) strong cell-cell adhesion (2000). (c) Radially expanding interface with weak (10) and (d) strong adhesion (2000). All interfaces have overhangs. Scaling analysis was done using overhang-corrected interfaces [14]. For the units, see Table S1.

factor [Eq. (6)]. Both scaling functions suggest KPZ dynamics; using the Family-Vicsek relation for the structure factor, Eq. (6) [Figs. 3(a) and 3(b)], and width, Eq. (1), the data collapse to a single function using the KPZ exponents [Fig. 3(d)]. The chi-squared statistics [Eq. (S12)] and goodness-of-fit p values indicate better collapse for the KPZ than for the MBE exponents (see Tables S2–S5).

Figure S1 shows that interface roughness $w(t)$ follows a power law t^{β} with $\beta^{\text{weak}} = 0.28 \pm 0.01$ and $\beta^{\text{strong}} = 0.25 \pm 0.02$ for weak and strong adhesion, respectively. Figures S2 and S3 show the local and global roughness exponents. As the figures show, determining the roughness exponent is questionable especially in the case of weak adhesion. The value $\alpha_{\text{loc}}^{\text{strong}} = 0.62 \pm 0.02$ was calculated using width,

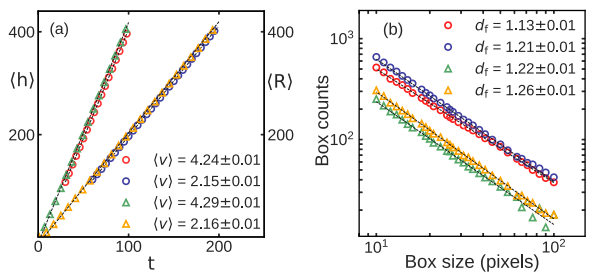

FIG. 2. (a) Velocity ($\langle v \rangle$) of the interface determined from the mean colony radius $\langle R \rangle$ and the mean interface height $\langle h \rangle$ vs time for different cell-cell adhesion strengths. Radially expanding interface: (red circles) at weak (10) and (blue circles) strong adhesion (2000). Line configuration: (green triangles) at weak and (orange triangles) at strong adhesion. (b) The fractal dimension (d_f) determined by plotting box counts vs box size. For radially expanding interface: (red circles) at weak (10) and (blue circles) strong adhesion (2000). For line configuration: (green triangles) at weak and (orange triangles) strong adhesion. For units, see Table S1.

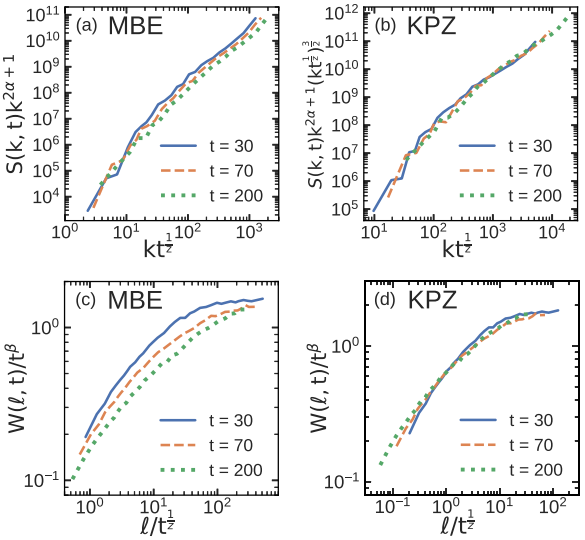

FIG. 3. Data collapse for line growth at high adhesion at three different times. (a) Using the structure factor [Eq. (6)] and MBE exponents, $\alpha^{\text{MBE}} = \frac{3}{2}$ and $z^{\text{MBE}} = 4$. (b) With KPZ exponents, $\alpha^{\text{KPZ}} = \frac{1}{2}$ and $z^{\text{KPZ}} = \frac{3}{2}$. The y axis is scaled with the factor $(kt^{\frac{1}{z}})^{\frac{3}{2}}$ to have the same range as MBE scaling. (c) Using the Family-Vicsek relation for width [Eq. (1)] with MBE exponents, $\beta^{\text{MBE}} = \frac{3}{8}$ and $z^{\text{MBE}} = 4$, and (d) with KPZ exponents, $\beta^{\text{KPZ}} = \frac{1}{3}$ and $z^{\text{KPZ}} = \frac{3}{2}$. For units, see Table S1.

and $\alpha_{\text{glob}}^{\text{weak}} = 0.75 \pm 0.04$ and $\alpha_{\text{glob}}^{\text{strong}} = 0.52 \pm 0.02$, using the structure factor. As the results show, α_{glob} decreases with increasing adhesion.

Next, we focus on radially expanding isotropic fronts. The initial configuration was one cell at the center of the simulation box and the final populations were ≈200 000 cells. We define $R_i(t)$ to be the distance from the center of mass of the colony to the ith site at the interface. Snapshots at different times and adhesion strengths are shown in Fig. 1; increasing the adhesion between the cells changes the colony morphology and increases overhangs. The radii grow at constant velocities, $\langle v \rangle = 4.24 \pm 0.01$ for weak and $\langle v \rangle = 2.15 \pm 0.01$ for strong adhesion [Fig. 2(a)]. As in the linear case, increasing the adhesion causes the front velocities to decrease. Again, the fractal dimension [Fig. 2(b)] shows a slight increase with increasing adhesion, $d_f^{\text{weak}} = 1.13 \pm 0.01$ and $d_f^{\text{strong}} = 1.21 \pm 0.01$.

Figures 4(a)–4(d) show the scaling results for radial growth both through the width function [Eq. (1)] and structure factor [Eq. (6)]. Using the Family-Vicsek relation for width [Fig. 4(c)] with MBE exponents displays good collapse. In addition, the structure factors at different times show good collapse with MBE exponents (see Tables S6–S9).

Figure S4 shows that fitting the width versus time gives the growth exponents $\beta^{\text{weak}} = 0.40 \pm 0.04$ and $\beta^{\text{strong}} = 0.42 \pm 0.06$, For varying adhesion strengths, the local roughness exponents α_{loc} are all within the same range: $\alpha_{\text{loc}}^{\text{weak}} = 0.66 \pm 0.01$ and $\alpha_{\text{loc}}^{\text{strong}} = 0.7 \pm 0.01$ (Fig. S5). The scaling exponent α_{glob}, measured from the structure factor, shows a decrease with increasing adhesion strength, $\alpha_{\text{glob}}^{\text{weak}} = 0.95 \pm 0.04$ and $\alpha_{\text{glob}}^{\text{strong}} = 0.71 \pm 0.02$ (Fig. S6).

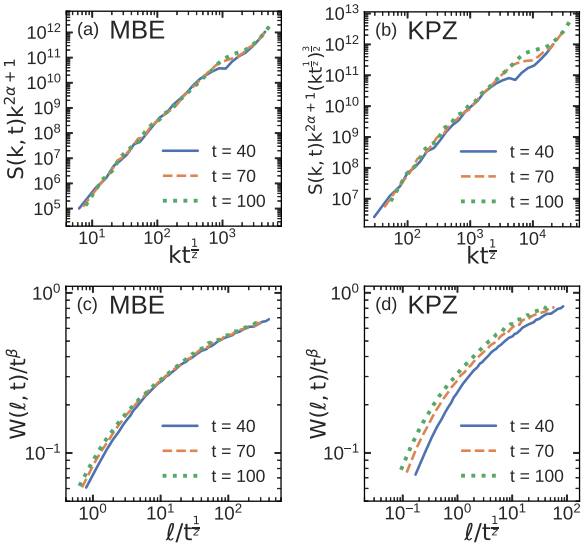

FIG. 4. Data collapse for the radially growing interface at low adhesion at three different times. (a) Using the structure factor [Eq. (6)] with MBE, $\alpha^{\mathrm{MBE}} = \frac{3}{2}$ and $z^{\mathrm{MBE}} = 4$ and (b) KPZ exponents, $\alpha^{\mathrm{KPZ}} = \frac{1}{2}$ and $z^{\mathrm{KPZ}} = \frac{3}{2}$. The y axis is scaled with the factor $(kt^{\frac{1}{z}})^{\frac{3}{2}}$ to have the same range as MBE scaling. (c) Using the Family-Vicsek relation for width [Eq. (1)] with MBE exponents, $\beta^{\mathrm{MBE}} = \frac{3}{8}$ and $z^{\mathrm{MBE}} = 4$, and (d) with KPZ exponents, $\beta^{\mathrm{KPZ}} = \frac{1}{3}$ and $z^{\mathrm{KPZ}} = \frac{3}{2}$. For units, see Table S1.

Finally, to test the generality of the above observations, cell-medium friction, intermembrane friction, cell division rules, and the number of cell types with different stiffness were tested using the radially growing system. Figure S7 shows that α_{glob} is insensitive to changes in factors such as cell-medium friction, intermembrane friction, cell division rules, and the number of cell types with different stiffness. These results suggest that the dynamics of the radially growing colonies are well described by MBE-like scaling when at weak cell-cell adhesion.

Conclusions. Our simulations indicate that weak cell-cell adhesion and an isotropically growing colony display MBE-like scaling for the boundary roughness. This is consistent with the experiments of Brú *et al.* [7]; we digitized their data and show its scaling in Fig. S8. In contrast, a colony growing from a single line of cells, and with strong cell-cell adhesion displays KPZ-like scaling. This is in agreement with the experiments of Huergo *et al.* [10]. In all the studied cases the fractal dimensions of the interface are within the range 1.13–1.26, which is also consistent with prior experiments [7,10,11,20,21], regardless of the growth scaling behavior.

All the studied cases show linear growth with constant velocity. This is consistent with experiments: Brú *et al.* reported radially spreading cell colonies to exhibit exponential growth in the early stages followed by linear growth [7]. Huergo *et al.* showed that once the number of cells exceeds 700–1000, radially spreading colonies grow with a constant velocity [11,20]. Constant velocity also applies for line growth [10]. Physically, these data suggest that cells are partially contact inhibited and that most activity occurs within a limited band along the interface challenging the notion of Gomperzian growth of cancer [35]. Experiments by Costa *et al.* indicate that *in vitro* cultivated cells may exhibit sigmoidal growth [3].

Finally, it can be assumed that the first multicellular life forms were rather simple cell colonies. It is interesting to speculate that if cell-colony growth dynamics would be rigidly confined to a single universality class, adaptive evolution would likely be significantly harder in contrast to more versatile growth dynamics. This is consistent with earlier results in the sense that very rich growth behavior and diverse tissues appear with modest changes, and, e.g., nontrivial dependencies in initial conditions, nutrients, apoptosis, disorder, and mechanical forces from various sources cause changes in both quantitative and qualitative behaviors (see, e.g., Refs. [2,28,31,32,36]).

CELLSIM3D assumes that adhesion molecules are distributed uniformly over the cell surface. This is, however, not necessarily the case in real cells since cell polarity may affect their distribution and activity [37–39]. Polarized cells may exhibit directional differences in their mechanical properties and cell-cell interactions, which may influence the dynamics of tissue roughness. Work is in progress to address such issues.

Acknowledgments. We thank the Natural Sciences and Engineering Research Council of Canada (M.K.), Canada Research Chairs Programs (M.K.), and Western University's Science International Engagement Fund (M.M.) for financial support. Computational resources were provided by the Finnish Grid and Cloud Infrastructure FGCI, funded by the Academy of Finland, Grant No. 304973.

[1] S. SenGupta, C. A. Parent, and J. E. Bear, The principles of directed cell migration, Nat. Rev. Mol. Cell Biol. **22**, 529 (2021).

[2] T. Lecuit and L. Le Goff, Orchestrating size and shape during morphogenesis, Nature (London) **450**, 189 (2007).

[3] F. Costa, M. Campos, and M. da Silva, The universal growth rate behavior and regime transition in adherent cell colonies, J. Theor. Biol. **387**, 181 (2015).

[4] J. Li, S. K. Schnyder, M. S. Turner, and R. Yamamoto, Role of the Cell Cycle in Collective Cell Dynamics, Phys. Rev. X **11**, 031025 (2021).

[5] E. Khain and J. Straetmans, Dynamics of an expanding cell monolayer, J. Stat. Phys. **184**, 20 (2021).

[6] M. Radszuweit, M. Block, J. G. Hengstler, E. Schöll, and D. Drasdo, Comparing the growth kinetics of cell populations in two and three dimensions, Phys. Rev. E **79**, 051907 (2009).

[7] A. Brú, S. Albertos, J. Luis Subiza, J. L. García-Asenjo, and I. Brú, The universal dynamics of tumor growth, Biophys. J. **85**, 2948 (2003).

[8] A. Brú, J. M. Pastor, I. Fernaud, I. Brú, S. Melle, and C. Berenguer, Super-Rough Dynamics on Tumor Growth, Phys. Rev. Lett. **81**, 4008 (1998).

[9] A. Brú, S. Albertos, J. L. Subiza, J. L. Garcia-Asenjo, and I. Brú, Reply to comments by Buceta and Galeano regarding the article "The universal dynamics of tumor growth", Biophys. J. **88**, 3737 (2005).

[10] M. A. C. Huergo, M. A. Pasquale, A. E. Bolzán, A. J. Arvia, and P. H. González, Morphology and dynamic scaling analysis of cell colonies with linear growth fronts, Phys. Rev. E **82**, 031903 (2010).
[11] M. A. C. Huergo, M. A. Pasquale, P. H. González, A. E. Bolzán, and A. J. Arvia, Dynamics and morphology characteristics of cell colonies with radially spreading growth fronts, Phys. Rev. E **84**, 021917 (2011).
[12] F. Family and T. Vicsek, Scaling of the active zone in the Eden process on percolation networks and the ballistic deposition model, J. Phys. A: Math. Gen. **18**, L75 (1985).
[13] F. Family, Dynamic scaling and phase transitions in interface growth, Physica A **168**, 561 (1990).
[14] A.-L. Barabási and H. E. Stanley, *Fractal Concepts in Surface Growth* (Cambridge University Press, Cambridge, U.K., 1995).
[15] M. Kardar, G. Parisi, and Y.-C. Zhang, Dynamic Scaling of Growing Interfaces, Phys. Rev. Lett. **56**, 889 (1986).
[16] D. A. Kessler, H. Levine, and L. M. Sander, Molecular-beam epitaxial growth and surface diffusion, Phys. Rev. Lett. **69**, 100 (1992).
[17] S. Das Sarma, S. V. Ghaisas, and J. M. Kim, Kinetic superroughening and anomalous dynamic scaling in nonequilibrium growth models, Phys. Rev. E **49**, 122 (1994).
[18] J. Buceta and J. Galeano, Comments on the article "The universal dynamics of tumor growth" by A. Brú *et al.*, Biophys. J. **88**, 3734 (2005).
[19] F. T. Hoyos, R. B. Navarro, J. V. Villadiego, and M. Guerrero-Martelo, Geometrical study of astrocytomas through fractals and scaling analysis, Appl. Radiat. Isot. **141**, 250 (2018).
[20] M. A. C. Huergo, M. A. Pasquale, P. H. González, A. E. Bolzán, and A. J. Arvia, Growth dynamics of cancer cell colonies and their comparison with noncancerous cells, Phys. Rev. E **85**, 011918 (2012).
[21] J. Galeano, J. Buceta, K. Juarez, B. Pumarino, J. De La Torre, and J. Iriondo, Dynamical scaling analysis of plant callus growth, Europhys. Lett. **63**, 83 (2003).
[22] S. N. Santalla, J. Rodríguez-Laguna, J. P. Abad, I. Marín, M. del Mar Espinosa, J. Muñoz-García, L. Vázquez, and R. Cuerno, Nonuniversality of front fluctuations for compact colonies of nonmotile bacteria, Phys. Rev. E **98**, 012407 (2018).
[23] T. Vicsek, M. Cserző, and V. K. Horváth, Self-affine growth of bacterial colonies, Physica A **167**, 315 (1990).
[24] J. A. Bonachela, C. D. Nadell, J. B. Xavier, and S. A. Levin, Universality in bacterial colonies, J. Stat. Phys. **144**, 303 (2011).
[25] M. A. C. Huergo, N. E. Muzzio, M. A. Pasquale, P. H. P. González, A. E. Bolzán, and A. J. Arvia, Dynamic scaling analysis of two-dimensional cell colony fronts in a gel medium: A biological system approaching a quenched Kardar-Parisi-Zhang universality, Phys. Rev. E **90**, 022706 (2014).
[26] S. N. Santalla and S. C. Ferreira, Eden model with nonlocal growth rules and kinetic roughening in biological systems, Phys. Rev. E **98**, 022405 (2018).
[27] M. Block, E. Schöll, and D. Drasdo, Classifying the Expansion Kinetics and Critical Surface Dynamics of Growing Cell Populations, Phys. Rev. Lett. **99**, 248101 (2007).
[28] Y. Azimzade, A. A. Saberi, and M. Sahimi, Effect of heterogeneity and spatial correlations on the structure of a tumor invasion front in cellular environments, Phys. Rev. E **100**, 062409 (2019).
[29] A. Buttenschön and L. Edelstein-Keshet, Bridging from single to collective cell migration: A review of models and links to experiments, PLoS Comput. Biol. **16**, e1008411 (2020).
[30] P. Madhikar, J. Åström, J. Westerholm, and M. Karttunen, CellSim3D: GPU accelerated software for simulations of cellular growth and division in three dimensions, Comput. Phys. Commun. **232**, 206 (2018).
[31] P. Madhikar, J. Åström, J. Westerholm, B. Baumeier, and M. Karttunen, Coarse-grained modeling of cell division in 3D: Influence of density, medium viscosity, and inter-membrane friction on cell growth and nearest neighbor distribution, Soft Mater. **18**, 150 (2020).
[32] P. Madhikar, J. Åström, B. Baumeier, and M. Karttunen, Jamming and force distribution in growing epithelial tissue, Phys. Rev. Res. **3**, 023129 (2021).
[33] See Supplemental Material at http://link.aps.org/supplemental/10.1103/PhysRevE.106.L062402 for details of the code, model, methods, and parameters, which includes Refs. [40–60].
[34] https://github.com/SoftSimu/CellSim3D.
[35] A. K. Laird, Dynamics of tumor growth, Br. J. Cancer **18**, 490 (1964).
[36] D. T. Tambe, C. Corey Hardin, T. E. Angelini, K. Rajendran, C. Y. Park, X. Serra-Picamal, E. H. Zhou, M. H. Zaman, J. P. Butler, and D. A. Weitz, Collective cell guidance by cooperative intercellular forces, Nat. Mater. **10**, 469 (2011).
[37] D. G. Drubin and W. J. Nelson, Origins of cell polarity, Cell **84**, 335 (1996).
[38] M. T. Butler and J. B. Wallingford, Planar cell polarity in development and disease, Nat. Rev. Mol. Cell Biol. **18**, 375 (2017).
[39] J. P. Campanale, T. Y. Sun, and D. J. Montell, Development and dynamics of cell polarity at a glance, J. Cell Sci. **130**, 1201 (2017).
[40] A. Mkrtchyan, J. Åström, and M. Karttunen, A New Model for Cell Division and Migration with Spontaneous Topology Changes, Soft Matter **10**, 4332 (2014).
[41] F. van Roy and G. Berx, The cell-cell adhesion molecule E-cadherin, Cell. Mol. Life Sci. **65**, 3756 (2008).
[42] M. P. Stemmler, Cadherins in development and cancer, Mol. BioSyst. **4**, 835 (2008).
[43] C. D. Buckley, G. E. Rainger, P. F. Bradfield, G. B. Nash, and D. L. Simmons, Cell adhesion: More than just glue (review), Mol. Membr. Biol. **15**, 167 (1998).
[44] G. M. Edelman and K. L. Crossin, Cell adhesion molecules: Implications for a molecular histology, Annu. Rev. Biochem. **60**, 155 (1991).
[45] M. A. Wozniak, K. Modzelewska, L. Kwong, and P. J. Keely, Focal adhesion regulation of cell behavior, Biochim. Biophys. Acta, Mol. Cell Res. **1692**, 103 (2004).
[46] P. Murray, G. Frampton, and P. Nelson, Cell adhesion molecules, BMJ **319**, 332 (1999).
[47] G. M. Edelman, Cell adhesion molecules, Science **219**, 450 (1983).
[48] D. K. Schluter, I. Ramis-Conde, and M. A. J. Chaplain, Multi-scale modelling of the dynamics of cell colonies: Insights into cell-adhesion forces and cancer invasion from in silico simulations, J. R. Soc. Interface **12**, 20141080 (2015).
[49] S. van Helvert, C. Storm, and P. Friedl, Mechanoreciprocity in cell migration, Nat. Cell Biol. **20**, 8 (2018).

[50] M. P. Stewart, J. Helenius, Y. Toyoda, S. P. Ramanathan, D. J. Muller, and A. A. Hyman, Hydrostatic pressure and the actomyosin cortex drive mitotic cell rounding, Nature (London) **469**, 226 (2011).

[51] A. Mkrtchyan, A single cell based model for cell divisions with spontaneous topology changes, Ph.D. thesis, University of Western Ontario, 2013.

[52] S. J. Morrison and J. Kimble, Asymmetric and symmetric stem-cell divisions in development and cancer, Nature (London) **441**, 1068 (2006).

[53] J. Kimble and S. L. Crittenden, *Germline proliferation and its control (August 15, 2005)*, in WormBook, edited by The C. elegans Research Community, WormBook, doi/10.1895/wormbook.1.13.1, http://www.wormbook.org.

[54] Y. Imoto, Y. Yoshida, F. Yagisawa, H. Kuroiwa, and T. Kuroiwa, The cell cycle, including the mitotic cycle and organelle division cycles, as revealed by cytological observations, J. Electron Microsc. **60**, S117 (2011).

[55] F. Bosveld, O. Markova, B. Guirao, C. Martin, Z. Wang, A. Pierre, M. Balakireva, I. Gaugue, A. Ainslie, N. Christophorou, D. K. Lubensky, N. Minc, and Y. Bellaïche, Epithelial tricellular junctions act as interphase cell shape sensors to orient mitosis, Nature (London) **530**, 495 (2016).

[56] P. Sahlin and H. Jönsson, A modeling study on how cell division affects properties of epithelial tissues under isotropic growth, PLoS One **5**, e11750 (2010).

[57] The HDF5 Group, Hierarchical Data Format, version 5, http://www.hdfgroup.org/HDF5/ (1997).

[58] G. Besold, I. Vattulainen, M. Karttunen, and J. M. Polson, Towards better integrators for dissipative particle dynamics simulations, Phys. Rev. E **62**, R7611 (2000).

[59] P. Nikunen, M. Karttunen, and I. Vattulainen, How would you integrate the equations of motion in dissipative particle dynamics simulations? Comput. Phys. Commun. **153**, 407 (2003).

[60] A. Rohatgi, https://automeris.io/WebPlotDigitizer Webplotdigitizer: Version 4.5 (2021).